STUDENT JOURNAL OF PHYSICS

Multiphysics Design of the Double Quarter-Wave Resonator Separator

David Diaz[1], Alexander Plastun[2], Peter Ostroumov[3]

[1]Third Year Undergraduate (junior), Department of Physics, Stony Brook University, Stony Brook, NY, 11794

[2]Accelerator Physicist, Accelerator Systems Division, Accelerator Physics Department, Facility for Rare Isotope Beams, Michigan State University, East Lansing MI, 48824

[3]Accelerator Physics Department Manager, Accelerator Systems Division, Accelerator Physics Department, Facility for Rare Isotope Beams, Michigan State University, East Lansing MI, 48824

Abstract: The Facility for Rare Isotope Beams and its experimental systems are currently under construction. The RF deflector based on a Double Quarter-Wave Resonator (QWR) is being designed for separation of rare isotopes. This paper presents some aspects of a multiphysics design of the RF deflector. The resonator will consume 42 kW RF power in order to provide the required deflection of ion beams. Removal of the heat from the resonator is required to control its shape and dimensions since the resonator should always be in resonance with the beam. The resonator is supported by a six-strut system to minimize the offset between the resonator and beam axes. Two cooling design options of heat pipes were also implemented into the resonator electrodes to improve the heat flow and temperature distribution. The rest change in resonant frequency due to thermal expansion will be corrected by using tuners.

Keywords: FRIB, RF Deflector, Surface Currents, Thermal Expansion

1. INTRODUCTION

The Facility for Rare Isotope Beams (FRIB) is currently being constructed at Michigan State University and will replace the existing Coupled Cyclotron Facility [1]. The experimental systems of the facility are being upgraded. One of the experimental beamlines will be equipped with an RF deflector for separation of the rare isotope beam. The RF deflector is based on the Double Quarter-Wave Resonator (QWR), Figure 1. The electromagnetic field excited inside the cavity resonator creates surface currents which lead to RF power dissipation and temperature increase of the cavity electrodes. This increase in temperature causes thermal expansion which alters the geometry of the magnetic and electric fields.

diaz_davido@hotmail.com[1], plastun@frib.msu.edu[2], ostroumo@frib.msu.edu[3]

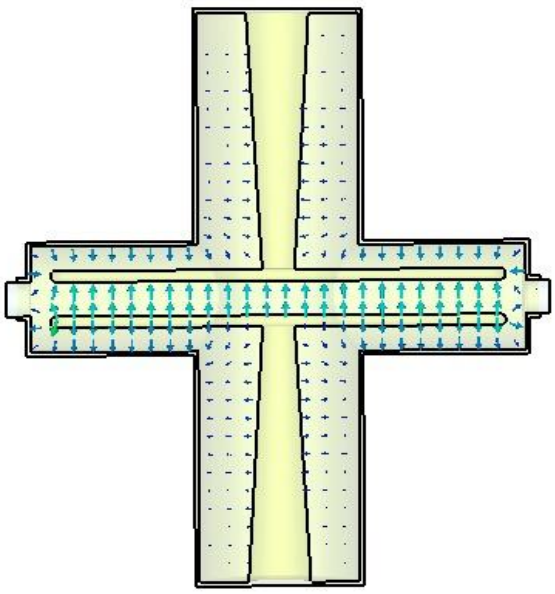

Figure 1. A cross section of the initial design for the QWR before any hermal management systems and nechanical supports are implemented. Here the electric field lines are being shown. The electric field that is produced in between the electrodes, capacitors, are due to the surface currents that are created when the cavity is in resonance. A magnetic field s also produced on the upper and ower parts of the cavity around the nner stems. The cavity is 3 meters high and 2.6 meters long.

Here is a way to understand the relation with resonance frequency change [2]:

$$\frac{\omega-\omega_0}{\omega_0}=\frac{\Delta U_m-\Delta U_e}{U_m+U_e} \tag{1}$$

where ω_0 is the initial resonance frequency of the unperturbed cavity, ω is the resonance frequency of the deformed cavity, U_m is the stored magnetic energy, and U_e is the stored electric energy. Eq. (1) shows how the change in magnetic and electric field energies are related to the change in resonance frequency. Creating the thermal management and mechanical support of the cavity would minimize the effects of thermal expansion and the optical axis offset. The following three equations show how thermal expansion affects the stored magnetic and electric energies:

$$\Delta L=L_0\alpha\Delta T \tag{2}$$

ΔL is the linear change in length of the electrodes and stems due to thermal expansion, L_0 is the original length of the material, α is the expansion coefficient of the material, and ΔT is the change in temperature of the material [3].

$$U_e=\frac{1}{2}\frac{\epsilon_0 A}{d}V^2=\frac{1}{2}CV^2, \tag{3}$$

where ϵ_0 is the permeability of free space, A is the planar surface area of each capacitor, d is the space in between the capacitors, C is the capacitance and V is the voltage [4].

(4)

$$U_m = \frac{B^2}{2\mu_0} AL,$$

Where μ_0 is the permittivity of free space, A is the cross-sectional area of the inductor, which is the stem, and L is the inductance [5].

The stored magnetic energy of the cavity is represented as an inductance because cavities can be modeled as RLC circuits. This specific cavity follows the path in Figure 2, where C_1 and C_2 are the capacitance between the electrodes and the tank, C_{coup} is the coupled capacitance between the electrodes, L_1 and L_2 are the equivalent inductance of the stems, and L_{coup} is the coupled inductance representing the current flow from one-half of the cavity to the other. You can see the circuit illustration of the QWR in Figure 2 below.

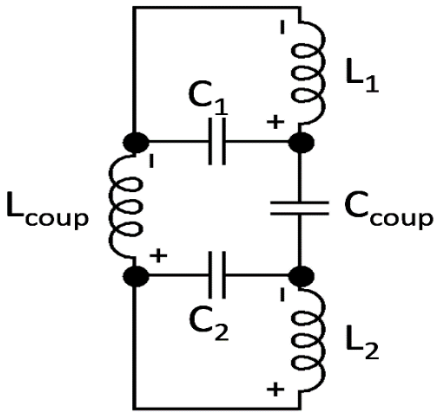

Figure 2. This is a sketch of the circuit representation of the double quarter wave resonator. Since, the cavity is able to be modeled in such a way, equations (2), (3), and (4) are sufficient enough to determine the change in resonance using equation (1).

2. DOUBLE QUARTER-WAVE RESONATOR SEPARATOR

The QWR is supposed to perform as an ion separator because of the RF electric field that is created in between the capacitors and oscillates at 20.125 MHz, Figure 1. The surface currents that are created go from one capacitor plate, up through its stem and around the cavity to the opposite stem and another capacitor plate. This path alternates in direction and so does the electric and magnetic fields. When an ion goes through the cavity, the electric field moves the ion in the ± $y^{¿}$ depending on its mass and RF phase. Plot 1 shows an example of $^{100}Sn^{50+}$ going through the cavity at the kinetic energy of 100 MeV/u, which results in an offset of approximately 14 mm near the end plane. This separation is important because a beam can contain many different particles and this will allow the separation of the beam depending on their arrival time to the cavity. Slits will be placed downstream the cavity to improve the purity of the beam. This ion motion simulation was performed with CST Particle Studio [6].

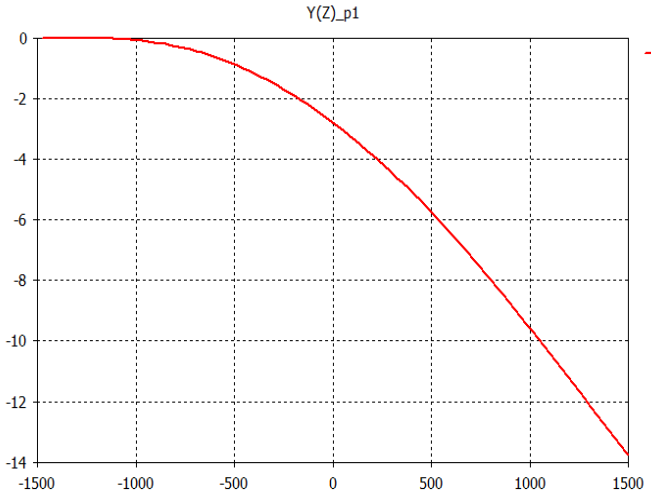

Plot 1. This is an example of $^{100}Sn^{50+}$ going through the cavity and acquiring an offset of approximately 14 mm from the optical axis. Both axes have the unit of mm and the cavity starts and ends at 1300 mm, respectively.

3. MULTIPHYSICS DESIGN

In order to minimize the thermal expansion, the temperature of the cavity needs to decrease. I used different approaches to cool the cavity. Different sections of the cavities produce different thermal losses, so the amount of cooling that is required can vary amongst different sections of the cavity. From the Thermal Solver in CST, I was able to determine the thermal losses in units of W/m^2, so to determine the overall thermal losses, I calculated the surface area of each section, i.e. stem, capacitor, and bases, and multiplied it by its average thermal loss in units of W/m^2.

The following table shows the power loss per section of the cavity:

Section	Units	Value
Top/Bottom Base	[W]	1333.5
Stem	[W]	14231.1
Top/Bottom Cylinder	[W]	3427.8
Top Part of Capacitor	[W]	1315.7
Bottom Part of Capacitor	[W]	218.4

Table 1. This shows the average values of thermal losses in the cavity due to resonance. The “Top Part” of the capacitor refers to the face that is farthest from the beam axis and the “Bottom Part” refers to the closest face.

The thermal losses shown in Table 1, drastically increase the temperature of the cavity, so the cooling channels and heat pipes were implemented.

3.1 Cooling Channels

The cooling channels on the outer tank surfaces all have a semi-circular cross section with a radius of 10 mm and a hydraulic diameter of 12.2 mm. These channels contain a water velocity of 1.0 m/s and a convection coefficient (h) of approximately 4500 W/m^2•K. The velocity can be adjusted to reach differing h values and change temperature distribution. All the helical and spiral cooling channels are represented as rings in the simulation to improve simulation speeds. This was also done to incorporate different reference temperatures to each ring to represent the water temperature increase along the channels, which makes the simulations more accurate.

The cooling channels in the stem are helical with a rectangular cross section of 10 mm x 10 mm and a pitch of 20 mm. The helical section of the cooling channel provides the most cooling to the stem, while the inner cylindrical channel, radius of 5 mm, is mainly for the entrance of the water flow. The water velocity is 2.5 m/s and it provides a convection coefficient of approximately 9000 W/m^2•K.

3.2 Heat Pipes

Not adding any thermal management to the capacitors’ plates proved to be very undesirable since a temperature gradient of 70 K is produced on the capacitors. Cooling channels were considered to thermally manage the capacitors. Simulating cooling channels in the capacitors provided a temperature distribution of less than 1 K in the capacitors, which would be ideal.

However, manufacturing of these cooling channels in the capacitors would be too difficult to make watertight while minimizing distortions on the surface of the capacitors. For this reason, I looked into heat pipes to see if these devices would be able to cool the capacitors. Heat pipes are used in many systems as thermal management and provides a watertight passive process, which would require less maintenance in the long run. Heat pipes have been used to improve the temperature distribution and heat flow in the capacitors. They are used to cause a temperature distribution of 2-5 K and have thermal conductivity that range from ten times to ten thousand times the thermal conductivity of copper [7]. Heat pipes are made out of a metallic shell, a complimentary liquid, a wick structure and a vapor space. They use the phase changes of condensing and vaporizing to cause an increase in the pipe's effective thermal conductivity. This is done by gaining energy to vaporize at the evaporator section and then release that as latent heat at the condenser section. The wick structure in the heat pipes allows for capillary movement of the liquid in the pipe to move from the condenser section to the evaporator section. These wick structures are made out of grooved edges in metal or with sintered metal. The following figure is a diagram to help visualize how a heat pipe functions:

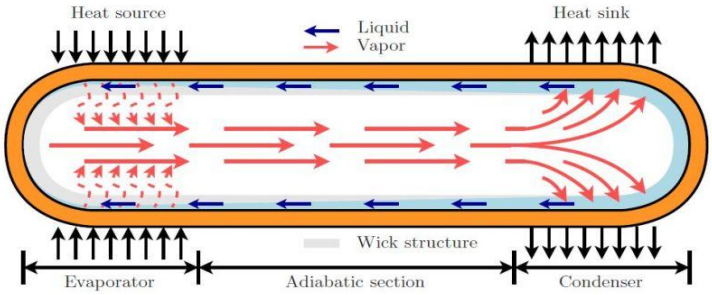

Figure 3. [8] This is a visual representation on the mechanics of a heat pipe as discussed in the text.

There are two designs for heat pipes in the capacitors with each heat pipe being cylindrical and encased in a 5 mm thick insulator, which can be seen in Figure 4. The insulator allows for 10 mm to be exposed on the condenser and evaporator sections of each heat pipe. The first design contains two sets of three parallel heat pipes, each 375 mm long, at each end of each capacitor, with the heat pipes closer to the stem being thicker due to the higher amount of heat flow. Heat pipes closer to the stem have a radius of 15.0 mm and the ones farther from the stem have a radius of 7.5 mm. The second design contains a set of three parallel heat pipes at each end of each capacitor with each pipe having a radius of 15.0 mm, but the center heat pipe would have a length of 800 mm and the ones on the sides would have a length of 400 m.

These designs were created to maximize heat flow and minimize the temperature distribution while maintaining more of a uniform distribution as opposed to having undesirable peaks.

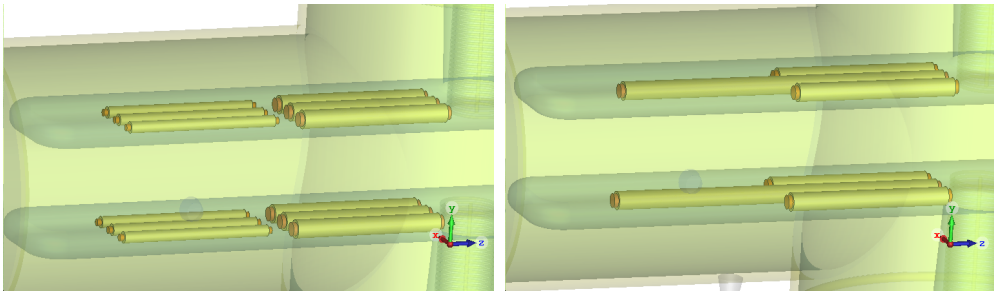

Figure 4. The left figure shows the first design of heat pipes that contains two sets of three parallel heat pipes partially surrounded by insulation. The right figure shows the second design of three parallel heat pipes of different sizes partially surrounded by insulation.

The heat pipes were simulated by creating a material similar to copper, except for its thermal conductivity which was varied to determine the right conductivity to create an accurate temperature distribution. After determining the thermal conductivity that creates a temperature distribution of 2-5 K, one has to check the power flow in the design center of Thermacore to see the limitations. This is done by noting the maximum and minimum heat flow that would be associated with each thermal conductivity. For the first design, the heat pipes closer to the stem had a thermal conductivity of 40,000 W/m·K and the heat pipes farther away had a thermal conductivity of 20,000 W/m·K. For the second design, all the heat pipes had a thermal conductivity of 40,000 W/m·K.

3.3 Six-Strut Support System

The mechanical support for the cavity is carried out by the six-strut system that is made to constrain an object's six degrees of freedom and minimize the optical axis offset. We followed some advice found from an article on how to implement the six-strut system to any object [9]. The struts are made orthogonally with one in $z^{¿}$, two in $x^{¿}$, and three in $y^{¿}$ directions, as seen in Figure 5.

The struts were designed in this way to provide the strongest constraint in the direction of most disturbances, which would be in the $y^{\dot{\iota}}$ in this case because of the additional vibrational disturbances from the floor. However, the lengths and positions of the struts can be altered to accommodate environmental restrictions.

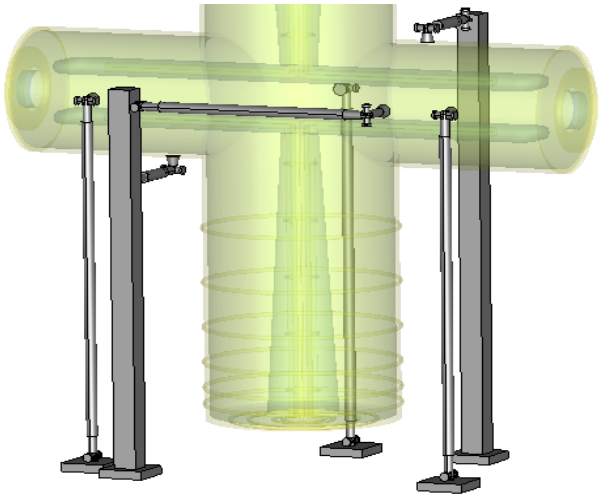

Figure 5. Here is a visual for the six-strut system implemented into the QWR multiphysics design. Here one can see what a strut looks like and how it is actually supposed to support the cavity as well as minimize the optical axis offset.

4. RESULTS

4.1 Thermal Results

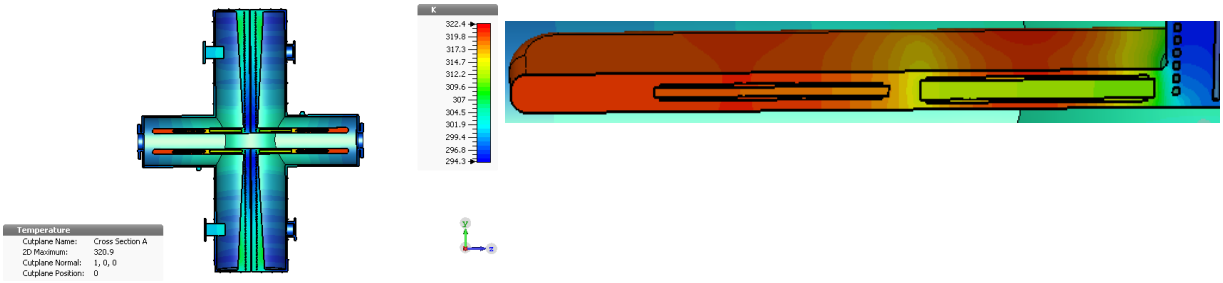

Figure 6. The temperature distribution for the first design of heat pipes. The bottom picture is an image zoomed to the surface of one of the capacitors to show the temperature distribution. The maximum temperature in the stem is 308 K and the maximum temperature in the capacitors is 322 K.

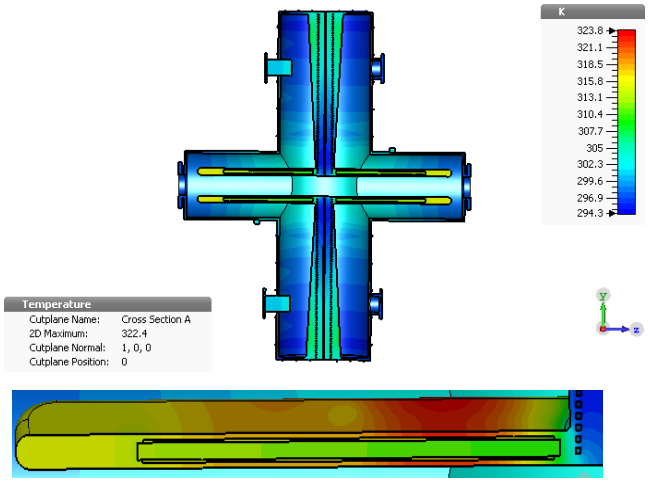

Figure 7. The temperature distribution for the second design of heat pipes. The bottom picture is an image zoomed to the surface of one of the capacitors to show the temperature distribution. The maximum temperature in the stem is 308 K and the maximum temperature in the capacitors is 324 K.

Figure 6 and Figure 7 show the temperature distributions that resulted from implementing cooling channels and heat pipes into the cavity. The temperature distributions are similar to each other and provide a much smaller temperature increase than before.

4.2 Results of Mechanical Analysis

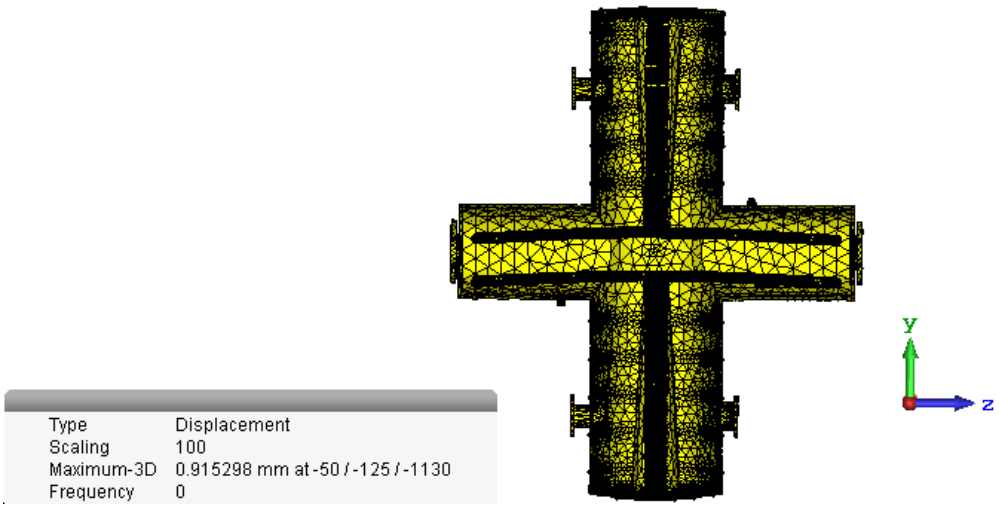

Figure 8. Deformation due to thermal expansion with the first design of heat pipes. These are deformations scaled 100 times. The drop at the capacitor's edges are due to gravity, also magnified 100 times.

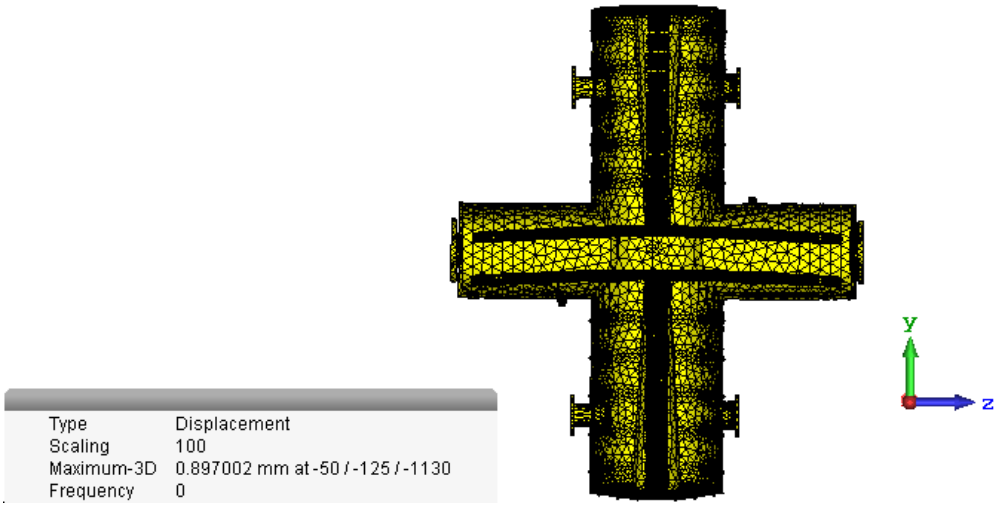

Figure 9. The deformation due to thermal expansion with the second design of heat pipes. These are deformations scaled 100 times. The drop at the capacitor's edges are due to gravity, also magnified 100 times.

Deformations due to thermal expansion with the temperature distributions in Figures 6 and 7 are shown in Figures 8 and 9. These deformations are scaled 100 times, so that they could be visible. The resulting deformations are very similar with slight variations, which results in similar changes in the resonance frequency. The change in the resonance frequency due to the first design is 5 kHz and the second design is 4 kHz. One main goal of the multiphysics design is to minimize the change in the resonance frequency, making it 0 if possible. However, the tuners implemented into the design on the upper and lower left of the cavity are movable to correct changes in resonance frequency up to approximately 20 kHz.

5. CONCLUSION

The final designs of the quarter-wave resonator separator include cooling channels, heat pipes, and a six-strut system. These designs differ by the structure of the heat pipes. However both the designs of the heat pipes result in a small change in the resonance frequency that can be corrected using tuners.

6. ACKNOWLEDEMENTS

I am grateful for the opportunity to conduct research at the Facility for Rare Isotope Beams through Michigan State University's Physics REU Program. I would also like to thank Peter Ostroumov for allowing me to work on this specific project and Alexander Plastun whose direct efforts and guidance allowed me to make such progress in my work.

References

[1] National Superconducting Cyclotron Laboratory, https://www.nscl.msu.edu/users/equipment.html

[2] Pozar, David M. Microwave Engineering. 4th ed. Hoboken, NJ: John Wiley & Sons, 2012.

[3] "Thermal Expansion," HyperPhysics, , accessed August 20, 2018, http://hyperphysics.phy-astr.gsu.edu/hbase/thermo/thexp.html.

[4] "Energy Stored on a Capacitor," HyperPhysics, , accessed August 20, 2018, http://hyperphysics.phy-astr.gsu.edu/hbase/electric/capeng.html.

[5] Boundless. "Boundless Physics." Lumen. Accessed August 20, 2018. https://courses.lumenlearning.com/boundless-physics/chapter/magnetic-fields-and-maxwell-revisited/.

[6] CST Particle Studio, https://www.cst.com/products/cstps

[7] Thermacore, https://www.thermacore.com/frequently-asked-questions/#70

[8] "Wits, IR. Wessel W., Dr. \"Two−Phase Heat Transfer Principles.\" University of Twente. Accessed July 27, 2018. https://home.ctw.utwente.nl/witsww/index.php/research/two−phase−principles."

[9] W. Thur, R. DeMarco, B. Baldock, K. Rex, in Proceedings of the 5th International Workshop on Accelerator Alignment, ANL/FNL Illinois, 1997, eConf C971013, IWAA (1997). http://www.slac.stanford.edu/econf/C971013/papers/045.PDF